

ORBITAL CHARACTERIZATION OF β PICTORIS B

H. Beust¹, G. Chauvin¹ and A.-M. Lagrange¹

Abstract. The young planet β Pictoris b offers the rare opportunity to monitor a large fraction of its orbit using the imaging technique over a reasonable timescale. Using NACO at VLT, we obtained repeated follow-up imaging observations of the β Pic system in the K_s and L' filters over 2010 and 2011. Together with past measurements, we have conducted an homogeneous analysis of data, that covers more than 8 yrs. We then derived the most probable orbital solutions that fit our measurements using a least-square algorithm and a Markov-Chain Monte Carlo approach. The solutions favor a low-eccentricity orbit $e \lesssim 0.2$, with semi-major axis between 8–11.5 AU corresponding to orbital periods of 15–25 yrs. Our solutions also favor highly inclined solution with a peak around $i = 88.5^\circ$ revealing a probable tilt with a perfectly edge-on configuration. We also derive prediction for transiting events. The solution is consistent with the planet being responsible for the 1981 transiting event. Finally, the planet seems compatible with former predictions linked with the cometary activity in the β Pic system.

Keywords: techniques: high angular resolution, stars: low-mass, brown dwarfs, stars: planetary systems

1 Introduction

Thanks to its probable moderate orbital period (~ 20 yrs), the recently imaged giant exoplanet β Pic b (Lagrange et al. 2009, 2010) offers a rare opportunity to rapidly constrain its orbital and physical properties, and connect them to the characteristics of the β Pic circumstellar environment.

Since the recovery of the planet (Lagrange et al. 2010), we have initiated an astrometric monitoring campaign, using NACO at VLT. In Sect. 2, we describe observations of 2010 and 2011 and we present our data analysis. In Sect. 3, we present the results of using a least-square algorithm and a Markov-Chain Monte Carlo approach. In Sect 4, we discuss the consequences of our results in the context of previous astrometric studies, and their implications regarding the previous indications for the presence of a giant planet orbiting β Pic.

2 Observations and data analysis

To pursue the monitoring of the β Pic b astrometry, we used the NaCo high contrast Adaptive Optics (AO) imager of the VLT-UT4 (Rousset et al. 2002; Lenzen et al. 2002). The follow-up observations were obtained at five different epochs between September 2010 and March 2011, using the angular differential imaging (ADI) mode of NaCo. For accurate astrometry, two observing set-ups were used, the L' filter with the L27 camera and the K_s filter with the S27 camera. The NaCo detector cube mode was in addition used for frame selection. At the end, the typical observing sequence represented a total of a 200–250 cubes, i.e, a total integration time of 35–50 min for an observing sequence of 1–1.5 hrs on target. A typical exposure time of 0.15s and 0.2s was respectively used in K_s and L' -filters to saturate the PSF core by a factor 100 (a few pixels in radius) to improve the dynamics of our images.

For the present study, we processed the data of the new observations of β Pic b obtained in September 28, 2010, November 16, 2010, November 17, 2010, February 1st, 2011 and March 26, 2011. Previous archived data including available astrometric calibrations, and obtained between November 2003 and April 2010, were also re-processed (see Table 1). The best astrometric measurements (in terms of observing conditions and stability)

¹ UJF-Grenoble 1 / CNRS-INSU, Institut de Planétologie et d'Astrophysique de Grenoble (IPAG) UMR 5274, Grenoble, F-38041, France

Table 1. NaCo astrometric measurements of β Pic b relative to β Pic

UT Date	Mode Obs/Filter/Obj	Platescale (mas)	True North (deg)	$\Delta\alpha$ (mas)	$\Delta\delta$ (mas)	separation (mas)	PA (deg)
10/11/03	Field/ L' /L27	27.11 ± 0.04	0.29 ± 0.07	233 ± 22	341 ± 22	413 ± 22	34.42 ± 2.82
25/10/09	Field/ L' /L27	27.11 ± 0.05	-0.08 ± 0.10	-153 ± 14	-257 ± 14	299 ± 14	210.74 ± 2.60
29/12/09	ADI/ L' /L27	27.10 ± 0.04	-0.06 ± 0.08	-163 ± 9	-260 ± 8	306 ± 9	212.07 ± 1.51
10/04/10	ADI/ K_s /S27	27.01 ± 0.04	-0.26 ± 0.09	-173 ± 7	-300 ± 7	346 ± 7	209.93 ± 1.26
28/09/10	ADI/ L' /L27	27.11 ± 0.04	-0.36 ± 0.11	-193 ± 11	-331 ± 11	383 ± 11	210.28 ± 1.57
16/11/10	ADI/ K_s /S27	27.01 ± 0.05	-0.25 ± 0.07	-207 ± 8	-326 ± 10	387 ± 8	212.41 ± 1.35
17/11/10	ADI/ L' /S27	27.10 ± 0.04	-0.25 ± 0.07	-209 ± 13	-330 ± 14	390 ± 13	212.34 ± 1.92
01/02/11	ADI/ K_s /S27	27.01 ± 0.04	-0.32 ± 0.10	-211 ± 19	-350 ± 10	408 ± 9	211.13 ± 1.33
26/03/11	ADI/ K_s /S27	27.01 ± 0.04	-0.35 ± 0.10	-214 ± 12	-367 ± 14	426 ± 13	210.13 ± 1.83

were kept at each epoch. Data obtained on November 16, 2010 and November 17, 2010 were both reduced to check the consistency of the results with both observing setups ($L'/L27$ and $K_s/S27$) used for this study.

The difficulty to derive the planet’s position relative to the star was to accurately estimate both the individual detector position of the saturated central star, and the planet position affected by the stellar residuals. We have fitted with a Moffat function the non-saturated part of the stellar PSF wing. To derive the planet position and flux, we used a grid of 5000 fake planets injected one-by-one in the data to derive the best solution minimizing the residuals in a region covering the companion ADI signature. The results are given in Table 1.

3 Orbital fit

a (AU)	P (yr)	e	i ($^\circ$)	Ω ($^\circ$)	ω ($^\circ$)	t_p (yr JD)	χ^2
11.2	28.3	0.16	88.8	-147.73	4.0	2013.3	5.37
8.8	19.6	0.021	88.5	-148.24	-115.0	2006.3	6.70

Table 2. Orbital solutions for β Pic b. **Top :** the best χ^2 model obtained with the LSLM algorithm; **bottom :** a typical “most probable” orbit according to the MCMC fit. Note that we do not give error bars here, as these are supposed to be described by the MCMC distribution.

We assumed for β Pic b an orbit described in a referential frame $OXYZ$ where the XOY plane corresponds to the plane of the sky, and where the Z -axis points towards the Earth. The position angle measurements (Table 1) are consistent with a quasi edge-on configuration of the orbit, which matches the position angle of the β Pic circumstellar disk (Olofsson et al. 2001). To best fit our measurements, we considered the planet’s inclination i as a free parameter.

A Keplerian model was fitted to our $(\Delta\delta, \Delta\alpha)$ results of Table 1 to constrain the orbital period P (or equivalently the semi-major axis a , using the stellar mass $M_* = 1.75 M_\odot$), the eccentricity e , the inclination i , the longitude of ascending node Ω (measured from North), the argument of periastron ω and the time for periastron passage t_p . We used two complementary fitting methods: a least-square Levenberg-Marquardt (LSLM) algorithm (Press et al. 1992) to search for the model with the minimal χ^2 , and a more robust statistical approach using the Markov-Chain Monte Carlo (MCMC) Bayesian analysis technique (Ford 2005, 2006).

The best LSLM χ^2 solution found, and a typical example of “most probable orbit” according to the result of the MCMC study, are given in Table 2. These orbits are plotted in Fig. 2, in a plane containing the line of sight, as well as the positions of the planet at various observing dates. The combined results of both fitting methods are also shown in Fig. 1. Surprisingly, the best LSLM model does not fall in the most probable peak, although this model obviously achieves actually the best χ^2 among our whole distribution. This discrepancy shows that our data are still too sparse to derive a deep χ^2 minimum. Consequently, our confidence in the LSLM approach must be low. This validates the MCMC approach, which better explores the parameter space. Considering the MCMC results, we first note that the semi-major axis is fairly well constrained by the fit. The most probable range is 8–11.5 AU (periods between 15–25 AU). Similarly, most eccentricities fall between 0 and ~ 0.17 . Solutions with higher semi-major axes and higher eccentricities cannot be completely excluded. They correspond to orbits with a periastron passage at ~ 9 AU to the SW side of the disk around 2009. Regarding the inclination, the

statistical distribution appears extremely concentrated close to 90° . The inclination nevertheless peaks at $\sim 88.5^\circ$, revealing a probable $\sim 1.5^\circ$ tilt with respect to a strict edge-on configuration. The statistical distribution of the argument of periastron ω is more erratic. Our results are in agreement with the orbital solution found by Currie et al. (2011) using a similar Monte Carlo technique, but using fewer data points. Interestingly, their results concerning the inclination are almost identical. Our semi-major axis range is nevertheless better constrained thanks to our extended data set.

4 Discussion

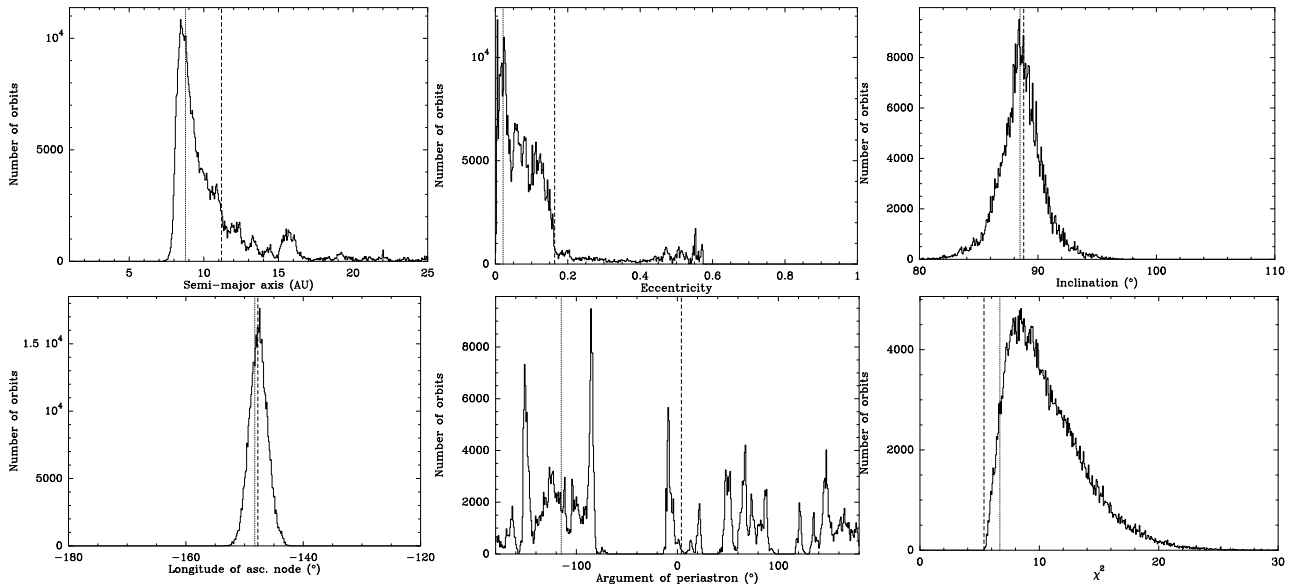


Fig. 1. Results of the MCMC fit of the astrometric data of β Pic b: statistical distribution of the orbital elements **Top left:** a ; **top middle:** e ; **top right:** i ; **bottom left:** Ω ; **bottom middle:** ω . **Bottom Right:** We also show the distribution of χ^2 of the solutions obtained. On each plot, the dashed line indicates the position of the best LSLM χ^2 model obtained, and the dotted line shows the position of the most probable orbit of Table 2.

From our previous orbital fit analysis, three important outcomes arise: the semi-major axis of β Pic b falls very probably in the range 8–11.5 AU, the eccentricity is most probably $\lesssim 0.2$, and the orbit is likely to have a $\sim 1.5^\circ$ tilt with respect to strict edge-on configuration. The existence of a giant planet orbiting β Pic had already been suggested by various previous studies. The main indirect signs pointed out are i/ the inner warped component of the β Pic circumstellar disk, together with additional asymmetries observed in the outer part (Mouillet et al. 1997; Kalas & Jewitt 1995), ii/ the photometric transit-like event observed in 1981 (Lecavelier des Etangs et al. 1997), and iii/ the cometary activity observed in the absorption spectrum of β Pic (Ferlet et al. 1987; Lagrange et al. 1996; Petterson & Tobin 1999). We discuss below how each of these observing facts may be related to the existence, and the orbital and physical properties of β Pic b.

4.1 Disk – Planet configuration

Dedicated scattered-light studies have accurately and morphologically detailed the view of the β Pic disk (Kalas & Jewitt 1995; Heap et al. 2000; Golimowski et al. 2006). They mainly show a nearly edge-on disk composed of a main disk observed beyond 80 AU, and an inner warped component (at less than 80 AU), and inclined by $2 - 5^\circ$ with respect to the main disk position angle. Simulations of Mouillet et al. (1997); Augereau et al. (2001) showed that the presence of a planet orbiting the star at 10 AU, misaligned with the main disk, could actually form and sustain the β Pic inner warped disk. (Currie et al. 2011) recently claimed evidence for a misalignment between the planet and the inner warped disk of β Pic concluding that the planet was orbiting inside the main disk’s orbital plane. We however do not confirm these results. This work and our $K_s/S27$ measurements of November 16, 2011 with a dedicated analysis for the disk orientation, shows that the projected separation of

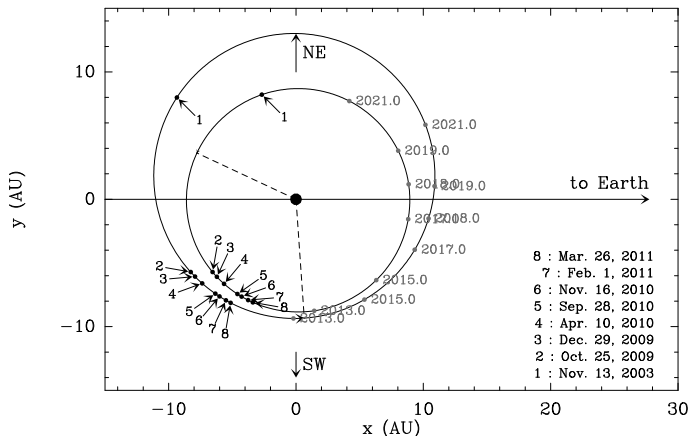


Fig. 2. Plots of the orbit of Table 2 with their orientation with respect to the line of sight. The larger orbit is the best LSLM χ^2 model and the smaller one is an example of most probable orbit obtained with the MCMC approach (Table 2). In each case, the dashed line shows the location of the periastron. The position of the planet at different observation epochs is shown as black dots along the orbit, and predictions for the upcoming years are shown in grey.

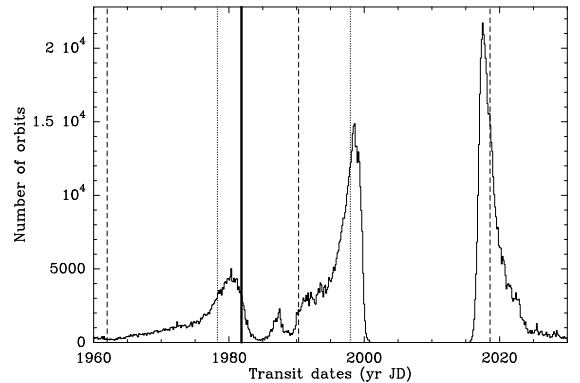


Fig. 3. MCMC distribution of the transit dates of β Pic b in front of the line of sight. The plotting conventions are the same as in Fig. 1. In addition, the date of the transit predicted by Lecavelier des Etangs et al. (1997) is marked with a thick vertical line.

β Pic b is actually located above the midplane of the main disk, supporting the planet being located in the warped component, and therefore being responsible for the inner warped morphology of the β Pic disk.

4.2 1981 Transiting event

Photometric follow-up of β Pic was made by Geneva observatory between 1975 and 1982. Lecavelier des Etangs et al. (1995) reports significant variations in November 1981 with a peculiar transit-like event on November 10, 1981. Lecavelier des Etangs et al. (1997) showed in that a planet with 2–4 times the radius of Jupiter, orbiting at ~ 9 AU at most could well be responsible for the photometric variations they report. Lecavelier des Etangs & Vidal-Madjar (2009) investigated this issue on the sole basis of the 2003 detection (Lagrange et al. 2009) of β Pic b. They found that a transit of β Pic b in November 1981 could be compatible with a quadrature position in November 2003, assuming a semi-major axis in the range [7.6–8.7] AU, without being able to definitely conclude. We reinvestigate this issue on the basis on our orbital fit. Figure 3 shows the MCMC distribution of the predicted transit dates of β Pic b between 1960 and 2030, assuming that the inclination is close enough to 90° to allow a transit of the clear zone around the planet at each orbit. We note that the most recent (~ 1999) and next (~ 2018) transits are somewhat well constrained. We also note a broader peak in ~ 1980 corresponding to the transit preceding the most recent one. The suggested transit date of November 1981 falls to the right edge in that peak (although not in the center). Therefore, the current orbital properties of β Pic b are still compatible with the planet being responsible for the 1981 transiting event.

4.3 The β Pic cometary activity

Transient redshifted spectral events have been regularly monitored in the absorption spectrum of β Pic (Ferlet et al. 1987; Lagrange et al. 1996; Petterson & Tobin 1999), and were attributed to the sublimation of numerous star-grazing planetesimals crossing the line of sight, also referred to as the Falling Evaporating Bodies (FEBs) phenomenon (Beust et al. 1996). Their origin was tentatively related to mean-motion resonances with a Jovian planet orbiting the star (Beust & Morbidelli 1996, 2000; Thébault & Beust 2001; Beust & Valiron 2007). Several constraints could be actually deduced from dynamical studies of the FEBs scenario, suggesting that: (i) The planet responsible for the phenomenon is massive enough (\sim Jovian) to allow numerous enough bodies to be trapped in the mean-motion resonances under consideration; (ii) its orbit is slightly eccentric ($e \gtrsim 0.05$ – 0.1) to allow bodies trapped in the resonances to see their eccentricity pumped up (Beust & Morbidelli 1996, 2000); (iii) the longitude of periastron of the planet with respect to the line of sight $m_{\text{was}} \sim -70^\circ \pm 20^\circ$ (Thébault

& Beust 2001), to enable the statistics of the Doppler velocities of the FEB spectral signatures to match the observed ones (strongly biased towards redshifts); (iv) the planet location was not further away than ~ 20 AU, otherwise the FEBs could hardly get into the dust sublimation zone.

The β Pic b planet has orbital and physical properties obviously compatible with constraints (i) and (iv). The situation is less straightforward for the constraints (ii) and (iii). Eccentricities larger than ~ 0.05 – 0.1 are actually fully compatible with our fit, but circular orbits are not excluded. Finally, the longitude of periastron ϖ measured from the line of sight is related to the argument of periastron ω from our fit. ω is measured from the XOY plane of our referential frame, i.e., the plane of the sky. Assuming an edge-on orientation of the disk, then we have $\omega = \varpi + \pi/2$. Thus $\varpi \simeq 70^\circ \pm 20^\circ$ means $\omega \simeq 20^\circ \pm 20^\circ$. Unfortunately, our constraint on ω is still too low to state whether this constraint is fulfilled or not. This is partly due to our still too weak constraint on the eccentricity itself. Further measurements are needed to refine this analysis.

5 Conclusion

We report the results of new follow-up observations of the astrometric positions of β Pic b relative to β Pic We then used to orbital fit techniques to derive the most probable orbital solutions for the β Pic b planet, including a least-square algorithm and Markov-Chain Monte Carlo Bayesian analysis. The latter approach gives us more robust and reliable results. The most probable solutions favor a low-eccentricity orbit $e \lesssim 0.2$, with semi-major axis between 8–11.5 AU corresponding to orbital periods of 15–25 yrs, and an inclination with a $\sim 1.5^\circ$ tilt with respect to strict edge-on configuration. The current orbital solution of β Pic b is consistent with the planet being responsible for the inner disk warp and the 1981 transiting event. Finally, it also supports β Pic b as the possible origin of the cometary activity observed in the β Pic system. Further deep imaging characterization should help reducing the orbital parameters space of β Pic b once the planet will have passed the next quadrature (most probably in 2013).

References

- Augereau J.-C., Nelson R.P., Lagrange A.-M., Papaloizou J.C.B., Mouillet D., 2001, *A&A* 370, 447
 Beust H., Lagrange A.-M., Plazy F., Mouillet D., 1996, *A&A* 310, 181
 Beust H. & Morbidelli A., 1996, *Icarus* 120, 358
 Beust H., Morbidelli A., 2000, *Icarus* 143, 170
 Beust H., Valiron P., 2007, *A&A* 466, 201
 Crida A., Masset F., Morbidelli A., 2009, *ApJ* 705, L148
 Currie T., Thalmann C., Matsumura S., et al., 2011, *ApJL*, 736, L33
 Ferlet R., Hobbs L.M., Vidal-Madjar A., 1987, *A&A* 185, 267
 Ford E.B., 2005, *AJ* 129, 1706
 Ford E.B., 2006, *ApJ* 642, 505
 Golimowski D. A., Ardila D. R., Krist J. E. et al. 2006, *AJ*, 131, 3109
 Heap S.R., Lindler D.J., Lanz T.M., et al., 2000, *ApJ* 539, 435
 Kalas P. & Jewitt D. 1995, *AJ* 110, 794
 Kalas P., Graham J.R., Chiang E., et al., 2008, *Science* 322, 1345
 Lagrange A.-M., Plazy F., Beust H., et al., 1996, *A&A* 310, 547
 Lagrange A.-M., Gratadour D., Chauvin G., 2009, *A&A* 493, L21
 Lagrange A.-M., Bonnefoy M., Chauvin G., et al., 2010, *Science* 329, 57
 Lecavelier des Etangs A., Deleuil M., Vidal-Madjar A., et al., 1995, *A&A* 299, 557
 Lecavelier des Etangs A., Vidal-Madjar A., Burki G., et al., 1997, *A&A* 328, 311
 Lecavelier des Etangs A., Vidal-Madjar A., 2009, *A&A* 497, 557
 Lenzen R., Hartung M., Brandner et al. 2002, *SPIE*, Vol. 4841
 Mouillet D., Larwood J.D., Papaloizou J.C.B., Lagrange A.-M., 1997, *MNRAS* 292, 896
 Olofsson G., Liseau R., Brandeker A., 2001, *ApJ* 563, 77
 Petterson O.K.L., Tobin W., 1999, *MNRAS* 304, 733
 Press W.H., Teukolsky S.A., Vetterling W.T., Flannery B.P., 1992, *Numerical Recipes* (Cambridge Univ. Press.)
 Rousset G., Lacombe F., Puget P., et al., 2002, *SPIE*, Vol. 4007
 Thébault P., Beust H., 2001, *A&A* 376, 621